Crystal Structure of ATP Sulfurylase from the Bacterial Symbiont of the Hydrothermal Vent Tubeworm *Riftia pachyptila*[†,‡]

John D. Beynon,[§] Ian J. MacRae,[||] Sherry L. Huston,[⊥] Douglas C. Nelson,[⊥] Irwin H. Segel,[||] and Andrew J. Fisher*[,§,||]

Department of Chemistry, Section of Molecular and Cellular Biology, and Section of Microbiology University of California, One Shields Avenue, Davis, California 95616

Received August 6, 2001; Revised Manuscript Received September 20, 2001

ABSTRACT: In sulfur chemolithotrophic bacteria, the enzyme ATP sulfurylase functions to produce ATP and inorganic sulfate from APS and inorganic pyrophosphate, which is the final step in the biological oxidation of hydrogen sulfide to sulfate. The giant tubeworm, *Riftia pachyptila*, which lives near hydrothermal vents on the ocean floor, harbors a sulfur chemolithotroph as an endosymbiont in its trophosome tissue. This yet-to-be-named bacterium was found to contain high levels of ATP sulfurylase that may provide a substantial fraction of the organisms ATP. We present here, the crystal structure of ATP sulfurylase from this bacterium at 1.7 Å resolution. As predicted from sequence homology, the enzyme folds into distinct N-terminal and catalytic domains, but lacks the APS kinase-like C-terminal domain that is present in fungal ATP sulfurylase. The enzyme crystallizes as a dimer with one subunit in the crystallographic asymmetric unit. Many buried solvent molecules mediate subunit contacts at the interface. Despite the high concentration of sulfate needed for crystallization, no ordered sulfate was observed in the sulfate-binding pocket. The structure reveals a mobile loop positioned over the active site. This loop is in a "closed" or "down" position in the reported crystal structures of fungal ATP sulfurylases, which contained bound substrates, but it is in an "open" or "up" position in the ligand-free *Riftia* symbiont enzyme. Thus, closure of the loop correlates with occupancy of the active site, although the loop itself does not interact directly with bound ligands. Rather, it appears to assist in the orientation of residues that do interact with active-site ligands. Amino acid differences between the mobile loops of the enzymes from sulfate assimilators and sulfur chemolithotrophs may account for the significant kinetic differences between the two classes of ATP sulfurylase.

ATP sulfurylase (sulfate adenylyltransferase, EC 2.7.7.4) catalyzes the transfer of the adenylyl group from ATP to inorganic sulfate (or from APS to inorganic pyrophosphate):

$$MgATP + SO_4^{2-} \rightleftharpoons MgPP_i + APS \qquad K_{eq} \approx 10^{-7}$$

This enzyme is ubiquitous although its physiological role depends on the metabolic lifestyle of the organism. In eukaryotes and many heterotrophic bacteria, ATP sulfurylase is used to generate APS[1] from inorganic sulfate and ATP. This is the first step in the conversion of inorganic sulfate to a variety of organic sulfur compounds including sulfate esters in animals and reduced sulfur-containing biomolecules in plants and microorganisms. Anaerobic sulfate reducing bacteria also use ATP sulfurylase to generate APS, but in these organisms, the APS serves as a terminal electron acceptor for the anaerobic respiration of organic compounds or H_2. In contrast to the above organisms, several classes of chemolithotrophic bacteria use ATP sulfurylase to produce ATP and sulfate from APS and pyrophosphate. That is, the physiologically important reaction in these organisms is in the opposite direction compared to that in sulfate assimilators and anaerobic sulfate reducers. The reaction is the final step in the overall oxidation of hydrogen sulfide, or other reduced inorganic sulfur compounds, to inorganic sulfate[2] and may be the sole substrate level phosphorylation in the energy-production pathway of these bacteria. With a reaction K_{eq} of 10^7 in the physiological direction and a K_m in the

[†] The research described in this report was supported by NSF Grant MCB-9904003 to I.H.S. and A.J.F., by NSF Grant EEP-9983119 and DOE Grant OE-FG03-00ER15077 to D.C.N., and by the W. M. Keck Foundation Center for Structural Biology at the University of California, Davis. J.D.B. and I.J.M. were supported by Public Health Service/NIH training Grant T32GM07377.

[‡] Protein coordinates have been deposited in the Protein Data Bank (file name 1JHD).

* To whom correspondence should be addressed. Phone: (530) 754-6180. Fax: (530) 752-8995. E-mail: fisher@chem.ucdavis.edu.

[§] Department of Chemistry.

[||] Section of Molecular and Cellular Biology.

[⊥] Section of Microbiology.

[1] Abbreviations: ATS, ATP sulfurylase; APS, adenosine 5′-phosphosulfate (adenylyl sulfate); PAPS, 3′-phosphoadenosine 5′-phosphosulfate (adenylyl sulfate 3′-phosphate); MgATP, $MgPP_i$, MgADP, magnesium complexes of the corresponding substrates or products; Tris, tris-hydroxymethylaminomethane; HEPES, *N*-2-hydroxyethylpiperazine-*N*-2′-ethanesulfonic acid; EDTA, ethylenediamine tetraacetate; MAD, multiple wavelength anomalous dispersion; RMSD, root-mean-square deviation; hp, hydrophobic amino acid residue. For brevity, "fungal" is used as a collective term when referring to the enzyme from both filamentous fungi and yeast. *Riftia* ATS refers to the enzyme from the bacterial symbiont of *Riftia pachyptila* (*not* the enzyme from the nontrophosome tissue of the animal.)

10.1021/bi015643l CCC: $20.00
Published on Web 11/07/2001

micromolar range for PP_i, the enzyme may provide the major route for recycling PP_i produced by biosynthetic reactions.

The deep-sea hydrothermal vents of the Pacific Ocean are an environment that is naturally abundant in hydrogen sulfide. H_2S issued from cracks in the ocean floor provides the energy source for chemolithotrophic bacteria that are present as endosymbionts in several invertebrate species. The giant tubeworm *Riftia pachyptila* is one such invertebrate. In place of a normal digestive track, the worm contains a trophosome tissue densely populated with an unnamed bacterium (*5*). The worm provides the symbiont with O_2 and CO_2 (via its hemoglobin) and the bacteria return reduced carbon compounds to the worm (*5*). ATP sulfurylase activity was reported to be present in the trophosome tissue 20 years ago (*6*). The enzyme was subsequently purified, kinetically characterized (*7*), and cloned (*8*).

To date, the only ATP sulfurylase crystal structures that have been reported are those from the filamentous fungus *Penicillium chrysogenum* (*9*) and the yeast *Saccharomyces cerevisiae* (*10*). Both organisms are sulfate assimilators, and both sulfurylases possess a common multidomain folding pattern. On the basis of sequence homology, we would expect ATP sulfurylase from the *Riftia* symbiont to adopt a fold similar to the N-terminal and catalytic domains of the *Penicillium* and yeast enzymes but to lack the C-terminal domain (which plays a regulatory role in the fungal enzyme). In fact, the native *Riftia* enzyme is a dimer with 396 residues/subunit (*7*), while the *Penicillium* and yeast enzymes are both hexamers with 573 and 521 residues, respectively. ATP sulfurylases from different types of organisms appear to have been optimized for their specific roles. For example, the Michaelis constants of the fungal enzymes for inorganic sulfate and MgATP (substrates for the physiological reaction) are 0.5−1 mM and ca. 0.2 mM, respectively, while the corresponding constants of the *Riftia* symbiont enzyme (where sulfate and MgATP are reaction products) are 27 and 1.8 mM, respectively. The *Riftia* symbiont enzyme also has a higher k_{cat} for the ATP synthesis direction (257 s^{-1} compared to 64 s^{-1} for the *P. chrysogenum* enzyme) (*7*). If early life on Earth existed in an environment similar to the deep-sea hydrothermal vents, it is possible that the enzyme from the *Riftia* symbiont resembles the primordial ATP sulfurylase from which this family of homooligomeric enzymes was derived.[3]

In this report, we present the crystal structure of ATP sulfurylase from the *Riftia* symbiont. This is the first structure of the enzyme from a chemolithotrophic organism to be elucidated. The results will contribute to our understanding of how subtle structural changes optimize the enzyme for its physiological function.

[2] In some sulfur chemolithotrophs, a different enzyme, APS: phosphate adenylyltransferase (originally called "ADP sulfurylase" after the reaction in the APS synthesis direction) may fulfill the same function (*1*). Certain *Thiobacillus* species contain both ATP sulfurylase and "ADP sulfurylase".

[3] Many Gram-negative bacteria contain a GTP-activated heterooligomeric ATP sulfurylase (*2*) that has little sequence homology to the homooligomeric enzymes present in filamentous fungi, yeast, algae, plants, animals, and some chemolithotrophs. Both the heterooligomeric and homooligomeric types may be present in some bacteria, e.g., *Allochromatium vinosum* (*3*).

EXPERIMENTAL PROCEDURES

Protein Expression and Crystallization. A 1.5 kb *Apo*I fragment from pBL20 (*8*) containing the gene of the *R. pachyptila* symbiont ATP sulfurylase was cloned into the *E*coRI site of pBluescriptSK$^+$ (Strategen, La Jolla, CA). The native protein was expressed in *Escherichia coli* using a clone with proper orientation of the T7 promoter and the inducible T7 RNA polymerase of pGP1−2 (*11*). A seleno-methionine-derivatized protein was produced by growing the same construct in a modified M9 minimal media (*12*). Methionine synthesis-inhibiting amino acids were added 20 min before induction and seleno-methionine was added at the beginning of the heat shock induction. Both native and seleno-methionine proteins were purified by ammonium sulfate precipitation (60−80% of saturation), DEAE anion-exchange column chromatography (0 to 1.5 M NaCl gradient), and finally Poros HQ (Perseptive Biosystems, Framingham, MA) anion-exchange column chromatography (0 to 1.0 M NaCl gradient). After purification (and between the above purification steps), the enzyme was dialyzed extensively against 10 mM Tris-Cl, pH 7.5, containing 0.2 mM EDTA. The enzyme was concentrated by membrane filtration to 30−50 mg/mL. Protein stocks diluted to 10 mg/mL were used for crystallization by hanging-drop vapor diffusion. A 1:1 dilution with precipitant was made and equilibrated against 2.3 M ammonium sulfate, 100 mM NaBr, and 2% PEG 400, 100 mM Na-HEPES, pH 7.5. The addition of 100 mM NaBr to the crystallization stock was found to be essential for reproducible crystallization. Crystals of the orthorhombic space group $P2_12_12$ grew over 2 weeks reaching a maximum size of 300 × 300 × 40 μm. Data collection showed unit cell parameters of $a = 59.56$ Å, $b = 75.55$ Å, and $c = 95.85$ Å with a V_M coefficient of 2.46 Å^3/Da (1 copy in the asymmetric unit) and a solvent content of 49.5% (*13*). Crystals were transferred to a cryo-protectant solution in three steps over 15 min. Each solution was identical to the mother liquor but contained, in order, 5, 10 and 15% glycerol. Crystals were cryocooled in a stream of nitrogen vapor at 100 K.

Data Collection and Phase Determination. Data sets were collected from two crystals on BL9-2 at SSRL. A three-wavelength MAD data set was collected on a seleno-methionine-derivatized protein crystal to 2.2 Å resolution. Dispersion and adsorption differences from the MAD data set provided the initial phase estimates. Data were also collected on the native protein to 1.7 Å at the bromide edge ($\lambda = 0.919\,70$ Å) in an attempt to identify ordered bromides. All data sets were processed with the programs DENZO and SCALEPACK (*14*). Twenty-two selenium sites were found in the MAD data set with SOLVE (*15*), resulting in an overall figure of merit 0.560. The experimental phases were improved by the maximum-likelihood solvent-flattening algorithm in RESOLVE (*16*, *17*), which increased the figure of merit to 0.600. Inspection of the flattened and unflattened electron maps showed only slight improvements in the already excellent experimental phases.

Model Building. Using the improved phases and the structure factors from the MAD data set, automated model building was initialed with ARP/wARP (*18*). Progress slowed after 200 cycles of refinement with 198 of the possible 396 residues built. The model after the 200th cycle of building was used as a starting model for further ARP/wARP

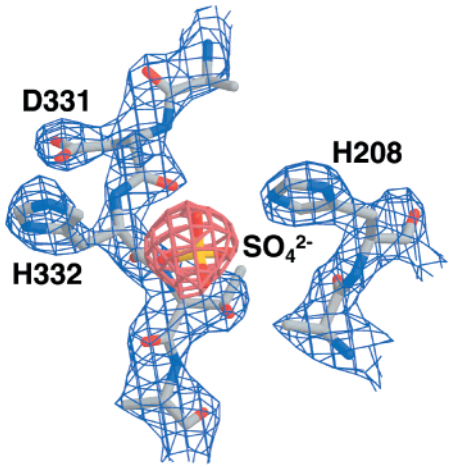

FIGURE 1: Representative section of the initial electron density map, calculated from experimental phases using MAD data collected at the Selenium edge. Shown in blue is the initial electron density corresponding to protein model built by ARP/wARP. The red region corresponds to the electron density of a sulfate ion. The sulfate density occupies the adenylyl ring-binding region. The map is calculated at 2.2 Å resolution and contoured at 1.5σ. This figure was drawn using the program BOBSCRIPT (*23*). Figures 2−7 were generated with MOLSCRIPT (*24*) and all figures were rendered with Raster3d (*25*).

automated building using the 1.7 Å resolution native data set. Automated model building of the native protein ended after 300 cycles with 374 of 396 residues built in five segments, all docked to the sequence. Most additional residues were built in the first 50 of the 300 cycles. The model was completed manually using the graphic program *O* (*19*). The main-chain density was clearly traceable through all 396 residues including the start codon methionine. CNS was used for energy minimization positional refinement, individual *B*-factor refinement, occupancy refinement of anions, and solvent building (*20*). Anomalous differences in the native data set were used to identify the bromide sites which ranged in intensity from 72 to 11 times sigma in the phased anomalous difference map. Sulfate sites were determined by visual inspection of electron density.

RESULTS

Overall Structure. The initial 2.2 Å resolution electron density map, calculated from phases using MAD data collected at the Selenium edge, produced a clean map that was readily interpretable (Figure 1). The electron density map was fitted using the automated model building routine implemented in the program ARP/wARP (*18*). After extending the resolution to 1.7 Å resolution, the program was able to fit all but 22 residues of the sequence, which were built manually. The final model contains all 396 residues of the bacterial *Riftia* symbiont ATP Sulfurylase including the N-terminal Met 1. The average *B*-factor for all non-hydrogen atoms in the refined model is 19.8 Å^2, which agrees well with the Wilson plot *B*-factor of 17.7 Å^2. The final conventional *R*-factor and *R*-free of the reported refined model are 16.7 and 20.5%, respectively. A total of 318 (or 92.7%) of the nonglycine and nonproline residues reside in the most-favored region of the Ramachandran plot, while the remaining 25 residues plot to the additionally allowed region. The crystallographic data and refinement statistics are summarized in Table 1. The orthorhombic crystals of *Riftia* symbiont ATP Sulfurylase contain 1 subunit/asymmetric unit. This subunit is situated next to the crystallographic 2-fold along the *c* axis to form the biologically functional dimer (*7*). Each subunit is ~75 Å in the largest dimension and varies from 44 to 48 Å in the other two dimensions.

Table 1: Data Collection, Phasing, and Refinement Statistics

	native (Br inflection)	Se-Met (peak)	Se-Met (remote)	Se-Met (inflection)
wavelength (Å)	0.919 70	0.979 23	0.885 60	0.979 42
resolution limit (Å)	1.7	2.2	2.2	2.2
no. of reflections	153 993	74 128	73 452	73 195
no. unique	46 914	22 472	22 375	22 500
completeness (%)	95.9 (71.6)	97.6 (83.9)	97.2 (79.9)	97.7 (85.0)
R_{merge}[a]	0.036 (0.163)	0.093 (0.355)	0.075 (0.360)	0.064 (0.357)
no. of sites	8	22	22	22
figure of merit		0.600		

Refinement Statistics

resolution (Å)	30−1.7
no. of reflections ($F \geq 0$)	46 914
R-factor[b]	16.7 (20.7)
R_{free}[b]	20.5 (27.7)
RMSD bond length (Å)	0.019
RMSD bond angles (°)	1.9

Asymmetric Unit Content

	no.	avg *B* (Å^2)
nonhydrogen protein atoms	3078	17.8
water	498	32.2
sulfates	3	22.7
bromides	8	27.4

[a] $R_{merge} = [\sum_h \sum_i |I_h - I_{hi}| / \sum_h \sum_i I_{hi}]$ where I_h is the mean of I_{hi} observations of reflection *h*. Numbers in parentheses represent highest resolution shell. [b] *R*-factor and $R_{free} = \sum ||F_{obs}| - |F_{calc}|| / \sum |F_{obs}| \times 100$ for 95% of recorded data (*R*-factor) or 5% of data (R_{free}). Numbers in parentheses represent highest resolution shell.

The *Riftia* ATS retains the overall structure and topology of the N-terminal and catalytic domains found in the *P. chrysogenum* (*9*) and *S. cerevisiae* (*10*) enzymes, but lacks the APS kinase-like C-terminal domain (Figures 2 and 3). The N-terminal domain (residues 1−172) contains a highly contorted mixed 5-strand β-sheet that is twisted into a partial β barrel and surrounded by α-helices. The catalytic domain spans residues 173−331 and is composed of a 5 strand parallel β-sheet surrounded by α-helices. Residues 332−396 form a subdomain consisting of a small three-strand β-sheet followed by two α-helixes. These residues associate with the main portion of the catalytic domain, but do not participate in the core β-sheet. A similar subdomain is present in the fungal structures (*9*, *10*).

Ion Binding. In the final structure, eight bromide ions were identified by inspection of the anomalous difference Fourier map. One Br^- stood out with a peak height of 72σ and was found buried between the core catalytic domain and the C-terminal subdomain where it interacts with polar groups of His 205 and Ser 379 and the hydrophobic side chains of Val 364, Leu 368, Val 383, and Leu 387. Of the seven other bromide ions ordered in the electron density map, their environment varied from highly solvated to buried in hydrophobic pockets.

Three sulfates are present in the final model. Two, which are located in the active-site region (but not at the catalytically relevant sulfate subsite) are discussed in more detail below. The third sulfate is found far from the active site in

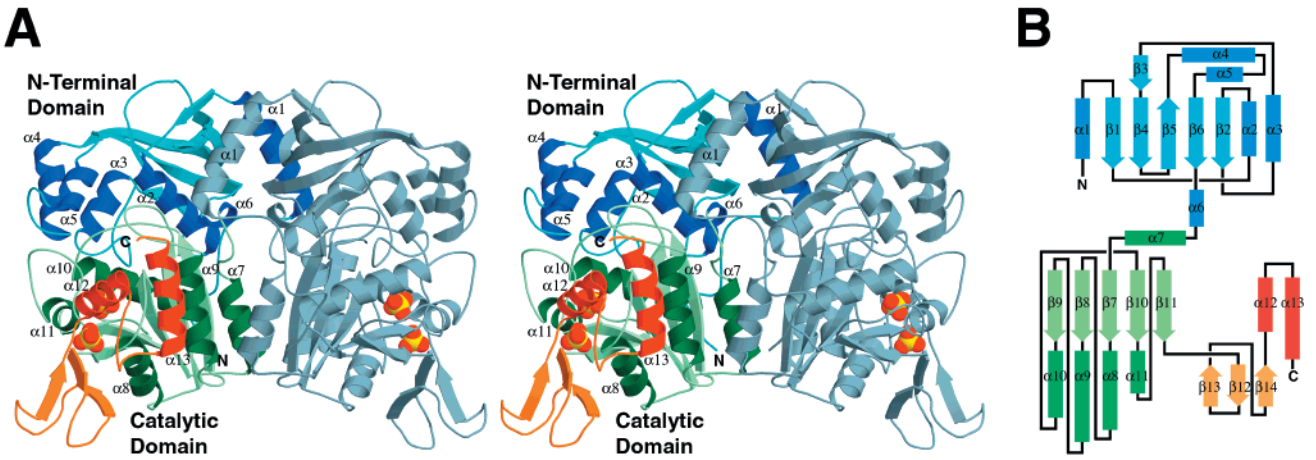

FIGURE 2: Structure of *Riftia* ATP sulfurylase. (A) Stereoribbon drawing of the enzyme. The crystallographic 2-fold axis is vertical in the plane of the page. This axis relates one subunit with colored domains to the other subunit shown in gray. The N-terminal domain is colored with different shades of blue. The catalytic domain can be divided into two subdomains shown in green and red, respectively. The two sulfate ions that bind near the active-site pocket are shown as CPK. (B) Schematic topology drawing of one *Riftia* ATS subunit. The color scheme is the same as in panel A.

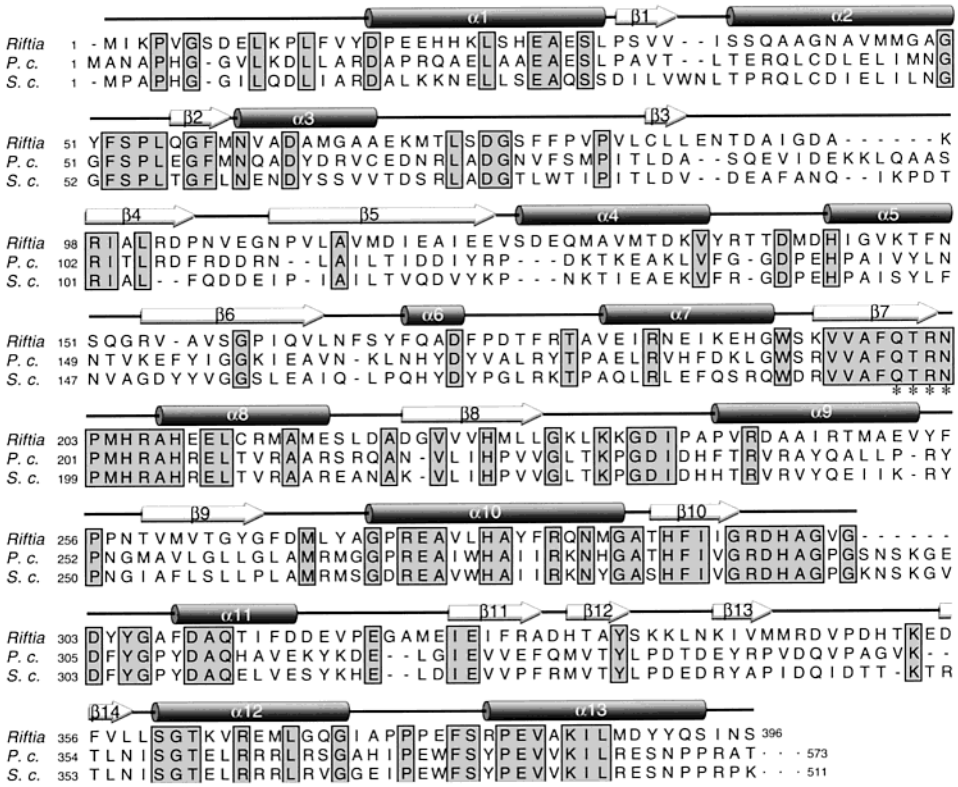

FIGURE 3: Primary sequence alignment of ATP Sulfurylase from the bacterial *Riftia* symbiont (*Riftia*) and the fungal; yeast *S. cereviseae* (*S. c*) and *P. chrysogenum* (*P. c.*) enzymes are shown with the corresponding secondary structure as observed in the *Riftia* crystal structure. The structural elements are indicated as follows: Cylinder = helix, arrow = β strand, line = loop or coil, there were no disordered sections of protein. Residues that are conserved in all three species are shaded. The asterisks (*) identify the conserved ^{199}QTRN phosphosulfate-binding pocket. Both fungal enzymes have an extended C-terminal domain not shown.

a salt-link to Lys 11 and within hydrogen-bonding distance to the main-chain nitrogens of residues Asp 8 and Glu 9.

ATP sulfurylase from the anaerobic, sulfate-reducing *Desulfovibrio* genus contains cobalt and zinc (*21*). Cadmium (from the crystallization medium) was observed in the yeast ATP sulfurylase structure and was suggested to play a functional role (*10*). However, no divalent metals were seen in either the *Penicillium* (*9*) or *Riftia* ATP sulfurylases. Moreover, the latter enzyme retained full activity after extensive dialysis against EDTA.

Dimer Organization. The dimerization surface of the *Riftia* ATP sulfurylase is similar to the interface between two of the catalytic domains found in the hexameric fungal ATP Sulfurylases (*9*, *10*). However, in the *Riftia* enzyme dimer, one monomer is rotated ~90° relative to the orientation in fungal ATS (Figure 4). Additionally, the *Riftia* dimer buries significantly more surface area compared to the fungal catalytic dimer, (1576 Å^2 compared to 332 Å^2 in the fungal enzymes). Despite the difference in protein orientation at the dimer interface, the *Riftia* dimer contacts across the interface

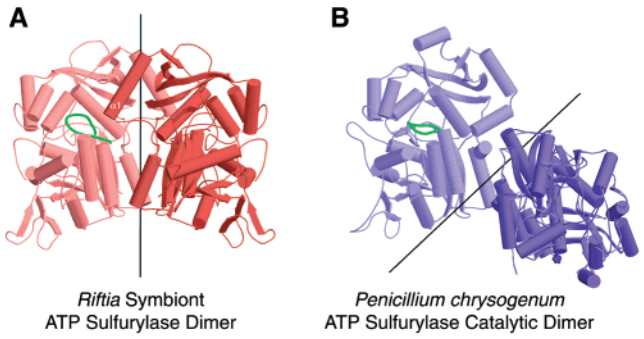

FIGURE 4: Dimer interface of *Riftia* and fungal ATS. Panel A illustrates the dimer formation of *Riftia* symbiont ATP sulfurylase as seen in the crystal structure. The different subunits are represented in different shades of red and the black line indicates the location of the crystallographic 2-fold axis that relates the two subunits in the *Riftia* enzyme. Panel B illustrates the fungal ATP sulfurylase catalytic dimer (as observed in the hexameric structure) with the left subunit (light blue) positioned in the same orientation as the *Riftia* (pink subunit in panel A). The two fungal ATP sulfurylase subunits are shown in different shades of blue with the C-terminal regulatory domain deleted for clarity. The black vector shows the crystallographic 2-fold axis that relates the dimer partners within the fungal hexamer. The dimerization surfaces are similar in the *Riftia* and fungal enzymes, but the second fungal subunit is rotated approximately 90° with respect to the *Riftia* enzyme. This view reveals the proximity of *Rifta* mobile loop, shown in green in the left subunit (A), to helix α1 of the 2-fold related subunit. There is no equivalent helix in the fungal enzyme to influence the conformation of the loop also shown in green (B).

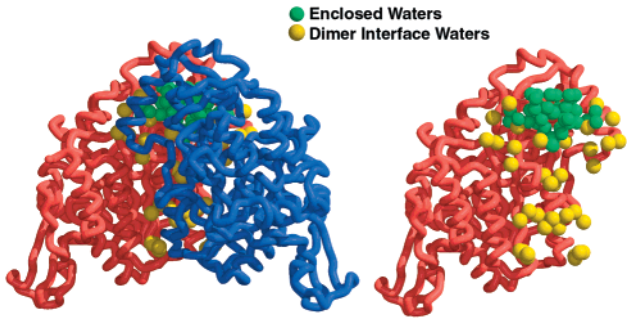

FIGURE 5: Water mediated dimer interface. (Left) ATP sulfurylase subunits are colored red and blue. Ordered solvent molecules that hydrogen bond to at least one atom in each subunit are shown in yellow. Ordered solvent molecules that reside in the dimer interface pocket formed by the N-terminal domain are shown in green. (Right) Same view and coloring as in left panel but with blue monomer removed for clarity.

resembles that of the catalytic−catalytic dimer interface within the hexameric structure of fungal ATS in that the majority of the interactions are through salt bridges or water-mediated hydrogen bonds. Dimer interactions in *Riftia* ATS are localized on and between helices α6 and α7, corresponding to residues 169−189 in fungal ATS. Additionally, some nonconserved residues on *Riftia* ATS helix α9 were found to interact with residues on helix α7 across the dimer interface. A common characteristic of both types of sulfurylases is the high level of solvation at the dimer interface (Figure 5). A total of 40 solvent molecules were found to mediate dimer interactions at the *Riftia* ATS dimer interface. Many salt-bridging residues across the dimer interface also interact with solvent molecules that act as bridges allowing additional dimer interactions. Two weak hydrophobic dimer interface interactions are specific to *Riftia* ATS: both Pro 18 and Pro 174 each interact with separate hydrophobic clusters on the symmetry related subunit. Additionally, a π-stacking motif extends across the dimer interface. The π stacking is centered on His 190 and its symmetry related mate; the imidazole rings are parallel and spaced 3.68 Å apart. The π-stacking pair of histidines is, in turn, sandwiched by Trp 192, 3.65 Å on either side. However, large hydrophobic patches commonly attributed to dimer interfaces are not observed.

An interesting feature of the dimer interface is a large solvent-filled pocket along the 2-fold axis formed by the N-terminal domain at the dimer interface (Figure 5). Helix α1 and strands β3, β5, and β6 line the pocket. The lip of the pocket is secured by a salt bridge between Glu 107 (on the hairpin loop between β2 and β3) and His 26 on α1 of the related monomer. The enclosure is accessible to bulk solvent along the 2-fold symmetry axis and through two small openings on each side, medial to the Glu 107−His 26 interaction. The pocket contains a total of 50 ordered solvent molecules.

Catalytic Site. Although *Riftia* ATS was crystallized in the presence of 2.3 M ammonium sulfate, no sulfate could be detected at the proposed catalytic site as was seen in the fungal enzymes (*9*, *10*). If sulfate were present at the active site, it would bind to the conserved ^{199}QXRN phosphosulfate motif. Specifically, one oxygen of the sulfate moiety would hydrogen bond to the Nϵ2 of Gln 199, another oxygen would salt-link to the Nη1 of Arg 201, and the third nonnucleophilic oxygen would hydrogen bond to the main-chain amide nitrogen of Ala 299 (Figure 6) (*9*, *10*). A preference of these H-bonding residues for electronegative oxygens might partly explain the high specificity of the enzyme for sulfate compared to phosphate. In the latter, the 3-fold H-bonded ion would position its un-ionized OH oriented toward the reactive α phosphoryl of ATP in a nonproductive complex. Additionally, the phosphate ion would have an additional negative charge compared to sulfate moiety, which would affect ion binding in the active site.

Two sulfate ions, however, were found in the active-site cleft near the sulfate-binding subsite, but the sulfates bind in a noncatalytic location (Figure 7). One sulfate binds between His 205 and His 208 of the conserved HXXH motif but does not hydrogen bond to either of these residues. (At its closest approach, one sulfate oxygen is 3.66 Å from Cδ2 of His 205.) Arg 365 holds the sulfate in position by forming two parallel hydrogen bonds between the two Nη atoms and two sulfate oxygens. The space occupied by this sulfate is in close proximity to that occupied by chlorate in the yeast enzyme (*10*). An oxygen of the other noncatalytic sulfate is 3.09 Å away from Cϵ1 of His 208 at a location known to accommodate the adenosine ring of nucleotide substrates in fungal ATP sulfurylase. This second sulfate hydrogen bonds with Oγ1 and the main-chain nitrogen of Thr 333 and with Nϵ2 of His 208 in addition to being well hydrated. The location of this sulfate may explain why soaking the crystals in solutions of $MgCl_2$ + ATP, APS, $MgCl_2$ + ATP + FSO_3^-, or the β-methylene analogue of APS did not produce a significant electron density in the active site. (The β-methylene analogue of APS was received as a generous gift from Prof. N. B. Schwartz, University of Chicago.) These noncatalytic sulfates (at least the one occupying the adenine pocket) are probably crystallization artifacts, because at millimolar assay concentrations—which approximate in vivo

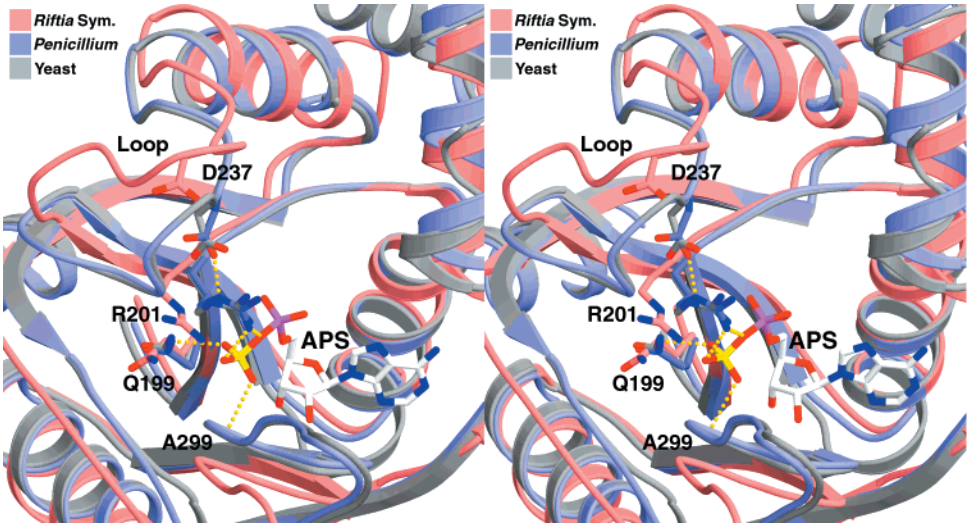

FIGURE 6: Superposition of the active sites from the three known ATP sulfurylase structures. Stereoview of the *Riftia* symbiont, *Penicillium*, and yeast active sites are shown in red, blue, and gray, respectively. APS, as observed in the *Penicillium* and yeast ATP sulfurylase structures, is shown with white carbon bonds. The mobile loop is in the open position in *Riftia* sulfurylase (red). In the fungal enzymes, the corresponding loops are in nearly identical "closed" conformations. Residues involved in sulfate or phosphosulfate binding are shown with numbering corresponding to the *Riftia* symbiont.

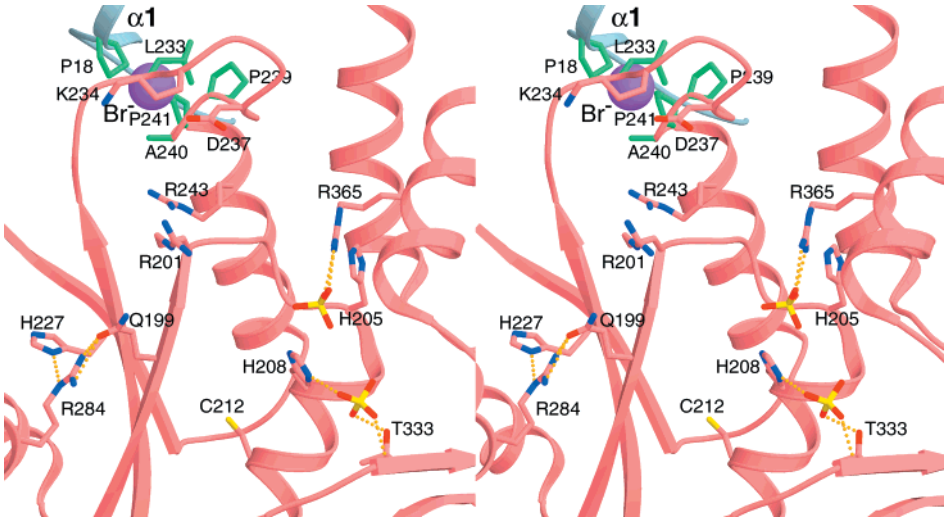

FIGURE 7: View of the active-site pocket and mobile loop of *Riftia* ATS. Sulfate did not bind in the sulfate binding pocket defined by residues Gln 199 and Arg 201 as was observed in the fungal enzymes. However, two sulfates did bind in the active-site region but not at the catalytically productive sulfate subsite. One sulfate bound between His residues 205 and 208, which are located close to the pyrophosphate binding region. Another sulfate bound between His 208 and Thr 333. The latter sulfate would sterically hinder entry of the adenylyl ring of ATP or APS. Residues shown in green reveal the hydrophobic interaction between residues in the mobile loop and the 2-fold related subunit (α1 shown in gray). Residues shown in pink carbon atoms are highly conserved in all sulfurylases and are involved in substrate binding and/or catalysis. Cys 212, whose modification in *Riftia* sulfurylase inactivates the enzyme, is also shown.

concentrations—sulfate does not exhibit substrate inhibition (*7*).

Mobile loop of the Active Site. A comparison of the *Riftia* with the fungal ATP sulfurylases reveals that the structure of the catalytic domain is highly conserved with an RMSD of 1.8 Å for 153 equivalent α-carbons spanning residues 173−331 (*Riftia* symbiont sequence numbering). The most notable difference between the catalytic domains, aside from the lack of APS in the *Rifta* ATS structure, is the different orientation of the loop composed of residues Gly 231 to Pro 241 (Figure 6). In the fungal structures, which contain bound substrates, this loop is folded over the catalytic site. *Penicillium* residue Asp 234 hydrogen bonds with the Nε of Arg 199, and Nη1 of this arginine coordinates an oxygen on the sulfate moiety of APS (*9*, *10*). In the *Riftia* ATS structure where the active site is vacant, this loop is rotated away from the active site. Thus, it is likely that the "closed" or "down" conformation of the loop is associated with active-site occupancy, while the "open" or "up" conformation is associated with ligand release from the active site. Flexibility of the loop is supported by the high *B*-factor observed for the *Riftia* structure but not for the fungal enzymes. Leu 230 in *Riftia* ATS and the equivalent Val 227 in *Penicillium* ATS appear to act as the N-terminal hinge of the mobile loop. The peptide bond of the *Riftia* Leu 230−Gly 231 and fungal Val 227−Gly228 hinge residues are flipped in opposite directions, which accounts for the divergent directions in the immediate downstream main chain. The basis of the loop movement at the C-terminal hinge is less defined but appears to involve a small tilt of helix α9. More flexible residues in the fungal ATP sulfurylase structures replace *Riftia* ATS residues Pro 239 and Pro 241. These Pro residues not only

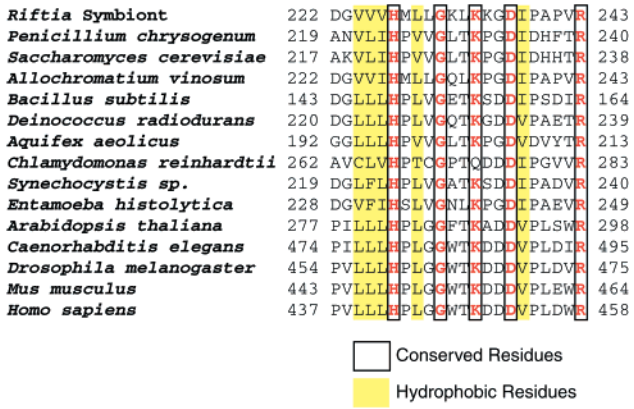

FIGURE 8: Sequence alignment of mobile loop region from 15 representative species. The invariant residues (with the exception of *Chlamydomonas reinhardtii*, Q substituted for K at position 274) are shown in red letters boxed in black outline. The conserved hydrophobic residues are shown with yellow background.

constrain the flexibility of the loop in *Riftia* ATS but also interact with the 2-fold related subunit through hydrophobic interactions. Leu 233, Pro 239, Ala 240, and Pro 241 from the loop along with Phe 173 from the same subunit interact with Pro 18 in α1 of the 2-fold related monomer to form a hydrophobic pocket at the dimer interface (Figure 7). This pocket appears to hold the loop open in the *Riftia* ATS structure. In the crystal structure, a bromide ion is centrally located in this hydrophobic pocket (Figure 7), but the ion is not responsible for holding the loop in the open position because the same loop conformation was observed in a structure solved from data collected from a crystal grown in the absence of Br^- (data not shown). The hydrophobic interactions that hold the loop open are not observed in the fungal structures. This difference may explain the low affinity for sulfate and the higher catalytic rate for ATP formation (i.e., for sulfate release) of the *Riftia* enzyme.

The mobile loop of *Riftia* ATS resides in a longer sequence which is highly conserved as ^{224}**(hp)$_3$HXhpXGXXKXX-Dhp**XXXX**R**^{243} among the diverse family of homooligomeric ATP sulfurylases (hp = hydrophobic residue) (Figure 8). (The residue following H is usually P, but it is M in the *Riftia* and *Allochromatium* enzymes.) The five invariant residues of the sequence provide clues to the catalytic mechanism of sulfurylase. For example, Nδ1 of His 227 hydrogen bonds with Nε and Nη2 of Arg 284. This interaction positions the latter to hydrogen bond to Gln 199 Oε1. As a result, Gln 199 Nε2 can only act as an H donor in the hydrogen bond formed with bound substrate, a feature that might explain the much higher affinity of the active site for sulfate compared to phosphate (see above). Gly 231 is located at the N-terminal hinge region of the loop and is likely conserved for its conformational flexibility, aiding in the rotation or flipping of the peptide bond with the preceding hinge residue accounting for the different conformations of the mobile loop. The structures of the fungal enzymes suggest that the carboxylate group of Asp 237 in *Riftia* ATS would orient Arg 201 through hydrogen bonds, allowing the latter to donate a hydrogen to the sulfate moiety if substrate were present in the active site. However, the carboxylate group of Asp 237 is ~7 Å away from the guanidinium group of Arg 201 in the "open" loop structure of *Riftia* ATS. Nη2 of Arg 243 in *Riftia* ATS is hydrogen bonded to the main-chain carbonyl oxygen of Arg 201. In the fungal structures, the homologue of Arg 243 hydrogen bonds to the main-chain carbonyl oxygen of the residue preceding the loop N-terminal hinge residue. The shifting of these hydrogen bonds may attenuate the movement of the flexible loop. Loop residue Lys 234 (and its fungal homologue) interacts only with solvent and is thermally energetic, as determined by their high *B* values. While the highly conserved active site does not allow for major substitutions, the mobile loop is much less conserved. The loop does not interact directly with substrate but rather, it orients residues that do bind the substrate. Thus, amino acid substitutions in the loop may cause small alterations in the orientation of active-site residues or in the kinetics of loop closing which "tunes" the catalytic features of the enzyme to the specific needs of the organism.

Structural Basis of Enzyme Inactivation by Thiol-Targeted Reagents. Riftia ATS is irreversibly inactivated by DTNB (*7*). The reactive cysteine was identified (by sequencing of a labeled tryptic peptide) as Cys 212 (unpublished results). Binding of APS, ATP, or sulfate protected against inactivation. The location of Cys 212 explains these observations. This residue is located adjacent to the nucleotide-binding site (Figure 7). Consequently, bound ATP or APS would effectively block the entry of an SH group-specific modifier. The Sγ of Cys 212 is 3.57 Å from His 208 of the HXXH motif, vital to the function of the enzyme (*22*). The Sγ is also 3.51 Å away from Phe 198, which is highly conserved among ATP sulfurylases and has been shown to make van der Waals contact with the ribose ring of the nucleotide (*9*, *10*). Any drastic movement in Phe 198 would also perturb other vital residues such as Gln 199 and Arg 201. Thus loss of function through modification of Cys 212 can be explained though the close proximity of these vital residues.

Comparison to Other ATP Sulfurylases. *Riftia* ATP sulfurylase shows 35 and 31% sequence identity, respectively, to the *Penicillium* and yeast sulfurylases over 394 aligned amino acid residues. The conserved residues in these comparisons are roughly evenly spread throughout the sequence, but with stretches of high conservation in areas that participate in substrate binding. A positional comparison of the full-length *Riftia* ATS and the *Penicillium* ATS gave an RMSD of 2.5 Å for 377 overlaid α-carbons (Figure 9). As expected (considering the different type of subunit interactions) the dimer interface has a relatively low level of sequence conservation. The catalytic domains retain the most similarity. The superposition of the *Riftia* ATP sulfurylase catalytic core domain (residues 173−331) overlays the *Penicillium* enzyme backbone with a RMSD of 1.8 Å. Divergence increases with increasing distance from the active site. The most obvious difference in the overlay is the movement of the mobile loop residue stretch 231−241 of the *Riftia* enzyme, compared with analogous residues 228−238 in the *Penicillium* enzyme.

DISCUSSION

Despite differences in the physiological function of sulfurylases from different organisms, the enzyme has retained a high level of homology from primordial *Riftia* ATS through the human enzyme. The residues that interact with the substrates are invariant. Therefore, to explain differences in kinetic properties we must look to diversity in the residues

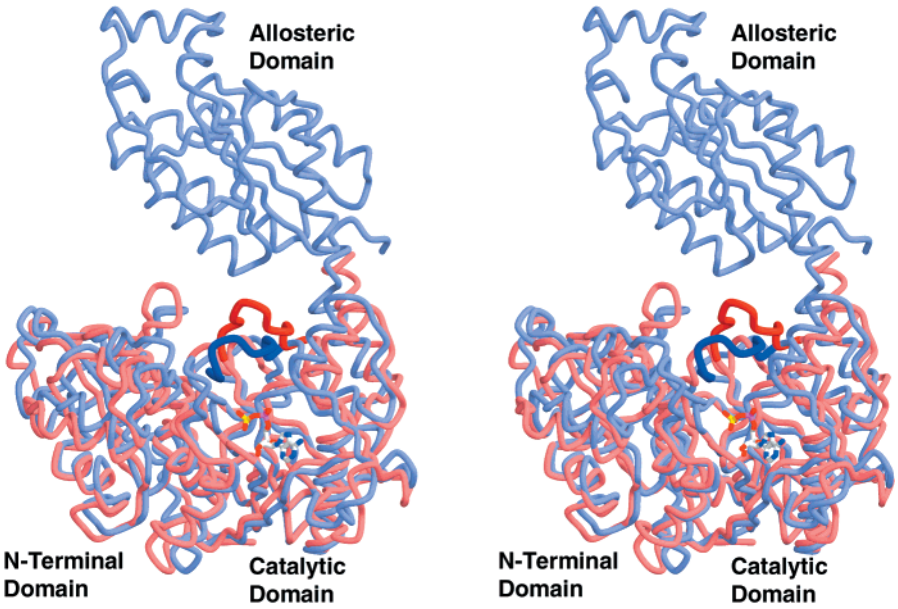

FIGURE 9: Stereoview showing the global overlay of *Riftia* (red) and *Penicillium* (blue) ATP Sulfurylase subunits (35% identity). The two structures superimpose with an RMSD of 2.5 Å for 377 equivalent α carbons. The *Penicillium* enzyme contains an additional C-terminal domain that allosterically modulates enzyme activity upon binding PAPS. The active-site mobile loop is highlighted in darker color. The loop corresponds to residues 231−241 in the *Riftia* enzyme and 228−238 in the fungal enzyme. APS, as observed in the *Penicillium* structure, is shown to identify the active site.

that aid in the positioning the catalytic residues. The loop composed of residues 231−241 may constitute such a "second layer" of active-site residues. The putative movement of the mobile loop has not been previously proposed, but in the reported structure of ATS from *P. chrysogenum*, APS was bound to the enzyme, and the loop was clearly located immediately over the active site (*9*). Similarly, the X-ray structures of yeast ATP sulfurylase with sulfate or APS or APS + PP_i bound at the active site (*10*) show the loop to be the "closed".

If, as the cumulative results suggest, the "closed" or "down" position of the loop stabilizes a sulfate-binding conformation of the active site, while the "open" or "up" position stabilizes a sulfate-release conformation, then evolutionary modifications to the region might underlie the catalytic differences between sulfurylases from sulfate assimilators and sulfur chemolithotrophs. That is, small changes in the flexibility and dynamics of loop movement may "tune" ligand binding, catalysis, and release of the substrates to the particular needs and environment of the host organism.[4] For example, the *Riftia* ATS dimer interface is equivalent to the catalytic domain dimer interface seen in the fungal hexamer. However, the 2-fold related *Riftia* subunit is rotated approximately 90° compared to the fungal 2-fold related subunit. This difference causes the mobile loop region to interact with α1 of the 2-fold related protein, an interaction that could help maintain an "open" conformation and thus, contribute to the lower affinity of the enzyme for sulfate. Of course, nonloop residues also participate in tailoring catalytic activity. For example, nucleotide binding to the yeast enzyme induces a large rotation of Phe 328 away from the adenine ring pocket (*10*). An analogous hydrophobic residue is not conserved in *Riftia* ATS.

[4] Changes in the distribution of enzyme molecules between the "open" loop and "closed" loop conformations may also underlie the T/R transition exhibited by allosteric ATP from filamentous fungi (*4*).

ACKNOWLEDGMENT

Portions of this research were carried out at the Stanford Synchrotron Radiation Laboratory, a national user facility operated by Stanford University on behalf of the U.S. Department of Energy, Office of Basic Energy Sciences. The SSRL Structural Molecular Biology Program is supported by the Department of Energy, Office of Biological and Environmental Research, and by the National Institutes of Health, National Center for Research Resources, Biomedical Technology Program, and the National Institute of General Medical Sciences.

REFERENCES

1. Bruser, T., Selmer, T., and Dahl, C. (2000) *J. Biol. Chem. 275*, 1691−1698.
2. Leyh, T. S., and Suo, Y. (1992) *J. Biol. Chem. 267*, 542−545.
3. Neumann, S., Wynen, A., Truper, H. G., and Dahl, C. (2000) *Mol. Biol. Rep. 27*, 27−33.
4. MacRae, I. J., Hanna, E., Ho, J. D., Fisher, A. J., and Segel, I. H. (2000) *J. Biol. Chem. 275*, 36303−36310.
5. Cavanaugh, C. M., Gardiner, S. L., Jones, M. L., Jannasch, H. W., and Waterbury, J. B. (1981) *Science 213*, 340−342.
6. Felbeck, H. (1981) *Science 213*, 336−338.
7. Renosto, F., Martin, R. L., Borrell, J. L., Nelson, D. C., and Segel, I. H. (1991) *Arch. Biochem. Biophys. 290*, 66−78.
8. Laue, B. E., and Nelson, D. C. (1994) *J. Bacteriol. 176*, 3723−3729.
9. MacRae, I. J., Segel, I. H., and Fisher, A. J. (2001) *Biochemistry 40*, 6795−6804.
10. Ullrich, T. C., Blaesse, M., and Huber, R. (2001) *EMBO J. 20*, 316−329.
11. Tabor, S., and Richardson, C. C. (1985) *Proc. Natl. Acad. Sci. U.S.A. 82*, 1074−1078.
12. Doublié, S. (1997) in *Methods in Enzymology* (C. W. Carter, J., and Sweet, R. M., Eds.) pp 523−530, Academic Press, New York.
13. Matthews, B. W. (1968) *J. Mol. Biol. 33*, 491−497.

14. Otwinowski, Z., and Minor, W. (1997) in *Methods in Enzymology* (Carter, J. C. W., and Sweet, R. M., Eds.) pp 307−326, Academic Press, New York.
15. Terwilliger, T. C., and Berendzen, J. (1999) *Acta Crystallogr., Sect. D 55*, 849−861.
16. Terwilliger, T. C. (1999) *Acta Crystallogr., Sect. D 55*, 1863−1871.
17. Terwilliger, T. C. (2000) *Acta Crystallogr., Sect. D 56*, 965−972.
18. Perrakis, A., Morris, R., and Lamzin, V. S. (1999) *Nat. Struct. Biol. 6*, 458−463.
19. Jones, T. A., Zou, J. Y., Cowan, S. W., and Kjeldgaard, M. (1991) *Acta Crystallogr., Sect. A 47*, 110−119.
20. Brünger, A. T., Adams, P. D., Clore, G. M., DeLano, W. L., Gros, P., Grosse-Kunstleve, R. W., Jiang, J.-S., Kuszewski, J., Nilges, M., Pannu, N. S., Read, R. J., Rice, L. M., Simonson, T., and Warren, G. L. (1998) *Acta Crystallogr., Sect. D 54*, 905−921.
21. Gavel, O. Y., Bursakov, S. A., Calvete, J. J., George, G. N., Moura, J. J. G., and Moura, I. (1998) *Biochemistry 37*, 16225−16232.
22. Venkatachalam, K. V., Fuda, H., Koonin, E. V., and Strott, C. A. (1999) *J. Biol. Chem. 274*, 2601−2604.
23. Esnouf, R. M. (1997) *J.Mol. Graphics Modell. 15*, 132−134.
24. Kraulis, P. J. (1991) *J. Appl. Crystallogr. 24*, 946−950.
25. Merritt, E. A., and Murphy, M. E. P. (1994) *Acta Crystallogr., Sect. D 50*, 869−873.

BI015643L